ARCHIVIO ISTITUZIONALE DELLA RICERCA

Alma Mater Studiorum Università di Bologna
Archivio istituzionale della ricerca

Viscosity of Palmas-type magmas of the Paraná Magmatic Province (Rio Grande do Sul State, Brazil): Implications for high-temperature silicic volcanism

This is the final peer-reviewed author's accepted manuscript (postprint) of the following publication:

Published Version:
Giordano, D., Vona, A., Gonzalez-Garcia, D., Allabar, A., Kolzenburg, S., Polo, L., et al. (2021). Viscosity of Palmas-type magmas of the Paraná Magmatic Province (Rio Grande do Sul State, Brazil): Implications for high-temperature silicic volcanism. CHEMICAL GEOLOGY, 560, 1-17 [10.1016/j.chemgeo.2020.119981].

Availability:
This version is available at: https://hdl.handle.net/11585/963209 since: 2024-02-28

Published:

DOI: http://doi.org/10.1016/j.chemgeo.2020.119981

Terms of use:

Some rights reserved. The terms and conditions for the reuse of this version of the manuscript are specified in the publishing policy. For all terms of use and more information see the publisher's website.

This item was downloaded from IRIS Università di Bologna (https://cris.unibo.it/).
When citing, please refer to the published version.

(Article begins on next page)

18 November 2024

Downloaded from http://sp.lyellcollection.org/ at Universidad Nacional Autonoma De Mexico on August 24, 2021

Accepted Manuscript

Geological Society, London, Special Publications

Evidence of the Early Holocene eruptive activity of Volcán de Colima and the 8.2 kyr global climatic event in lacustrine sediments from a debris avalanche-dammed lake

L. Capra, M. Roverato, J. P. Bernal & A. Cortés

DOI: https://doi.org/10.1144/SP520-2021-63

To access the most recent version of this article, please click the DOI URL in the line above. When citing this article please include the above DOI.

Received 30 March 2021
Revised 24 June 2021
Accepted 16 July 2021

© 2021 The Author(s). Published by The Geological Society of London. All rights reserved. For permissions: http://www.geolsoc.org.uk/permissions. Publishing disclaimer: www.geolsoc.org.uk/pub_ethics

Supplementary material at https://doi.org/10.6084/m9.figshare.c.5563424

Manuscript version: Accepted Manuscript
This is a PDF of an unedited manuscript that has been accepted for publication. The manuscript will undergo copyediting, typesetting and correction before it is published in its final form. Please note that during the production process errors may be discovered which could affect the content, and all legal disclaimers that apply to the book series pertain.

Although reasonable efforts have been made to obtain all necessary permissions from third parties to include their copyrighted content within this article, their full citation and copyright line may not be present in this Accepted Manuscript version. Before using any content from this article, please refer to the Version of Record once published for full citation and copyright details, as permissions may be required.

Downloaded from http://sp.lyellcollection.org/ at Universidad Nacional Autonoma De Mexico on August 24, 2021

Evidence of the Early Holocene eruptive activity of Volcán de Colima and the 8.2 kyr global climatic event in lacustrine sediments from a debris avalanche-dammed lake.

Capra[1*], L., Roverato[2], M., Bernal[1], J.P., Cortés[3], A.,

1. Centro de Geociencias, Campus UNAM-Juriquilla, 04510 Querétaro, Mexico.

2. Department of Earth Sciences, University of Geneva, Switzerland.

3. Centro Universitario de Estudios e Investigaciones de Vulcanología, Universidad de Colima, Colima, Col., Mexico.

ORCID ID: LC 0000-0003-3973-7264, MR: 0000-0001-5681-6218, JPB: 0000-0001-8363-572.

*Corresponding author (lcapra@geociencias.unam.mx)

Supplementary material: Table 1s. Major and trace elements of the Gypsum King sequence.

ACCEPTED MANUSCRIPT

Downloaded from http://sp.lyellcollection.org/ at Universidad Nacional Autonoma De Mexico on August 24, 2021

Abstract

Volcán de Colima, one of the most active volcanoes in Mexico, experienced at least nine flank failures during the last 30,000 years, with catastrophic effects on the environment that implies the formation of temporary dams where lacustrine sediments accumulated for hundreds of years. These lacustrine sequences preserve an exceptional record from which to reconstruct the effect of subsequent volcanic eruptions and, eventually, contemporary environmental and climatic conditions. Here we analyze an Early Holocene lacustrine sequence, named "Gypsum King", which accumulated in a short-lived temporary lake, likely formed by emplacement of the 10755-11230 cal. yr BP Mesa-Yerbabuena debris avalanche. Through detailed analysis of the 1.8 m thick lacustrine sequence (^{14}C ages, sulfur content, grain size), it was possible to identify the 8.2 kyr global climate event and better constrain the Early-Holocene main sub-plinian to plinian eruptions of Volcán de Colima. The results presented here highlight the potential to explore sulfur content and abrupt change in grainsize in lacustrine sediments as additional proxies to better constrain eruptive phases in volcanic environments. Finally, the Gypsum King sequence provides the first evidence of the 8.2 kyr global climate event along the Eastern tropical Pacific Coast.

Keywords

8.2 kyr global climate event; Intertropical Convergence Zone; volcanic lake; Plinian eruption, volcanic collapse, Volcán de Colima; Mexico.

1. Introduction

Lacustrine sedimentation in volcanic environments is commonly associated with crater lakes related to monogenetic volcanism and maars: volcanic diatremes filled with groundwater at the end of the eruptive phases. These lacustrine sequences can represent an undisturbed record that provides detailed information on local volcanological, ecological and climatic changes over thousands of years (i.e. Caballero et al., 2003; Mingram et al., 2004; Zolitschka et al., 2006). Other types of lakes can also form in volcanic environments, whose duration will depend on their origin and hydrological framework. This is because volcanic activity can almost instantaneously emplace large volumes of material that can interrupt main drainages, inducing the formation of natural impoundments (Fan et al., 2020). The best examples are associated with the emplacement of a debris avalanche deposit after volcanic edifice lateral collapse (Costa and Schuster, 1988; Tibaldi et al., 2005; Capra, 2007): some of which still persist since their formation, i.e. at Parinacota (Chile) or Iriga (Japan) where a hydrological balance was reached naturally or, as in the case of some of the lakes formed after the 1980 Mount St. Helens eruption, artificially (Costa and Schuster, 1991). Volcanic collapses are

ACCEPTED MANUSCRIPT

Downloaded from http://sp.lyellcollection.org/ at Universidad Nacional Autonoma De Mexico on August 24, 2021

recognized as a frequent event during the evolution of a stratovolcano, and lacustrine sedimentation is common after the emplacement of large debris avalanche deposits. These sediments can preserve important information that can allow the frequency of younger explosive eruptions to be established, especially in environments where erosion can rapidly erase stratigraphic records. Nevertheless, many former lakes in volcanic environments are now missing, and only their sediments remain, generally in the form of hanging sequences exposed in vertical terraces and intercalated with other volcaniclastic deposits. This phenomenon has been identified at Volcán de Colima, México (19.5° N, 103.6° W) (Figure 1a) where at least three temporary lakes were formed during the emplacement of debris avalanche deposits during the Late Pleistocene and Holocene (Capra and Macias, 2002; Cortes et al., 2010a). Here, in addition to the volcanological significance of the formation of temporary lakes during the emplacement of debris avalanches and the associated hazard, we present geochemical data with paleoclimatological implications obtained from a peculiar lacustrine sequence, here named Gypsum King (GK), discovered along the Los Ganchos ravine, a tributary ravine of the main Armeria River (Figure 1b). We present a detailed sedimentological description of the 1.8 m thick Gypsum King sequence and use new ^{14}C ages to correlate it with the Late Holocene explosive activity of Volcán de Colima, and provide evidence of the hydroclimatic effects of the 8.2 kyr global climate event in southwestern Mexico (Thomas et al., 2007).

2. The 8.2 kyr climatic event in Mexico

The 8.2 kyr event has been described as a global abrupt climatic change resulting from the outbursts of pro-glacial lakes Agassiz and Ojibway into the North Atlantic, which disrupted thermohaline ocean currents and caused cold and dry conditions in the North Hemisphere (Barber et al., 1999; Alley et al., 1997; Alley and Ágústsdóttir 2005). The event punctuated the relative thermal stability observed during most of the Holocene until pre-industrial times. One impact of this event was southward migration of the Intertropical Convergence Zone (ITCZ) (LeGrande et al., 2006; Morrill et al., 2013), resulting in a decrease in precipitation in Central America (Lachniet et al., 2004b), an increase in Amazonian precipitation, and suppression of the Indian and Asian summer monsoon (Cheng et al., 2009; Dixit et al., 2014). Evidence of this climatic event has been gathered from ice cores (Alley et al., 1997; Thomas et al., 2007), speleothems (Cheng et al., 2009), and marine and lacustrine sediments (Heard et al., 2007; Elison et al., 2006) that placed this event at *ca* 8.2 kyr and lasting ~ 200 years (i.e. Clarke et al., 2003). More detailed work identified two main peaks starting at 8.21 +/- 0.02 kyr and lasting 70 and 20 years respectively (Thomas et al 2007; Cheng et al., 2009).

In Mexico, palynological data and geomorphological observations from Iztaccíhuatl volcano (central Mexico; figure 1a) suggest that cold and dry conditions prevailed during the 8.2 kyr event (Lozano-

ACCEPTED MANUSCRIPT

Downloaded from http://sp.lyellcollection.org/ at Universidad Nacional Autonoma De Mexico on August 24, 2021

García and Vázquez-Selem, 2005; Vázquez-Selem and Heine, 2012). Paleoclimate reconstructions from southwestern Mexico support the prevalence of contemporaneous dry conditions, inferred from the abrupt interruption of stalagmite growth in Guerrero state (Bernal et al., 2011), and vegetation changes recorded in sediments from Lake Zirahuén (Lozano-Garcia et al., 2013). However, a detailed high-resolution reconstruction of the event is not yet available. This is particularly relevant, as records of the 8.2 kyr event in the eastern Pacific basin are scarce.

3. The Volcán de Colima

The Volcán de Colima, one of the most active volcanoes in Mexico, is located in the western sector of the Trans-Mexican Belt, and lies in the Colima graben, a tectonic depression whose margins of massive limestone (Tepames Formation) present a topographic barrier to volcaniclastic flows, increasing their tendency to obstruct the two main rivers that run along the graben margins, the Armeria to the west and the Naranjo to the east (Figure 1b and c). Following the 1913 plinian eruption, volcanic activity has been characterized by summit dome growth and collapse generating block-and-ash flow deposits up to 7-8 km from the crater, as occurred during the 2004-2005 crises and more recently in July 2015 (Macias et al., 2006; Capra et al., 2015; Macorps et al., 2018; Davila et al., 2019) with an extraordinary runout of 10.5 km. Recently, Crummy et al. (2019a,b), expanding the previous work of Luhr et al. (2010), reviewed the Late Pleistocene-Holocene eruptive activity of Volcán de Colima, based on a detailed analysis of main tephra fallout and pyroclastic surge deposits outcropping in proximal areas. They report more than 180 ^{14}C ages from samples collected in 89 localities across an area of ~ 500 km^2, grouping them in several volcanic units. In particular, the Early-Holocene stratigraphy (7000-8400 cal. yr BP) has been characterized by four main explosive periods named, from younger to older, Unit O, N, M and L. Unit O is characterized by 30, up to > 100 cm thick, sequences of multiple layers of tephra and pyroclastic surge deposits. Eleven radiocarbon dates from this unit allow it to be constrained to the interval between 6981-7171 cal. yr BP and 7587-7800 cal. yr BP (Table 1), representing ~ 700 years of intermittent explosive activity (Crummy et al., 2019a,b). Unit N (7779-8013 cal. yr BP) is a massive tephra fall up to 60 cm in thickness; Unit M (7776-8043 cal. yr BP) is characterized by 12 to 100 cm thick ash-rich deposits with lenses of tephra falls, and Unit L (8280-8402 cal. yr BP) consists of massive tephra fall deposits up to 50 cm in thickness. For all these eruptions, the main dispersal axis of tephra falls was towards the E-NE. However, based on the stratigraphic record, the most common and catastrophic activity of Volcan de Colima consisted of edifice collapses with the emplacement of debris avalanche deposits (DAD), as occurred at least 9 times during the past 30,000 years (Komorowski et al., 1997; Cortes et al., 2010b, 2019; Roverato et al., 2011; Roverato and Capra, 2013). These deposits extended up to 45 km to the south with volumes of up to 35 km^3 (Komorowski et al., 1997; Cortes et al., 2010b, 2019).

ACCEPTED MANUSCRIPT

Downloaded from http://sp.lyellcollection.org/ at Universidad Nacional Autonoma De Mexico on August 24, 2021

Detailed stratigraphic studies demonstrate that these deposits caused the temporary damming of the Naranjo and Armería rivers resulting in the accumulation of thick lacustrine sequences (Capra and Macias, 2002; Cortes et al., 2010a). During the Holocene, at least four edifice failures occurred: the younger 2425-2740 cal. yr BP El Remate-Armeria (ERA-DAD), the 3594-4242 cal. yr BP Los Ganchos (LG-DAD), the 7590-8172 cal. yr BP Villa de Alvarez Coquimatlán (VAC-DAD), and the 10755-11230 cal. yr BP Mesa Yerbabuena (MY-DAD) (Komorowski et al., 1997; Cortés et al., 2010a; 2010b; 2019) (Table 1.). In particular, the MY-DAD and VAC-DAD events are here discussed in detail as their emplacement are directly related to the GK lacustrine sequence.

4. Methods

The GK lacustrine sediment column was sampled at 5 cm intervals for grain size and chemical analyses. Five samples were collected for ^{14}C dating (C1, C2, C3, C4, C5) including bivalve shells from the bottom of the sequence (BS) and for ^{14}C analysis by BetaAnalytic (Table 1). The resulting ages were calibrated using Calib 8.2 (Stuiver et al., 2021) based on the IntCal20 Northern Hemisphere radiocarbon age-calibration (Reimer et al., 2020); all reported uncertainties correspond to 2σ. An age-model for the stratigraphic sequence was made based upon the 5 radiocarbon ages using Bacon (Blaauw and Christen, 2011). Ages for all the collected samples were calculated using the resulting age-model (Figure 2).

Major and trace element analysis was carried out by X-ray fluorescence spectrometry in fused $LiBO_2/Li_2B_4O_7$ disks, using a Rigaku PRIMUS WD-XRF spectrometer and a Rh-target. Samples were oven-dried overnight, weighed and mixed with a 1:1 $LiBO_2/Li_2B_4O_7$ mixture in a 1:9 sample:flux ratio and fused in a Claisse M4 automatic fluxer. Analysis of sulfur and other trace elements was also carried out using WD-XRF, but on pressed pellets using the semi-quantitative SQX software. Accuracy and precision were verified using IGL reference materials (Lozano and Bernal, 2005) (Table 2 and Table 1s). Grainsize distribution was determined with a laser sedimentograph (Fritsch Analysette 22) (Table 2).

5. Stratigraphic record and age of the Gypsum King lacustrine sequence.

Along the Los Ganchos ravine, up to 100 m-high terraces expose intercalated debris avalanche and lacustrine sequences, interrupted by thick volcaniclastic layers such as debris flows (lahars) and fluviatile horizons (Cortes et al., 2010a). At section LA1 (Figure 1c), ~22 km SW from the volcano summit, the outcrop consists of a 2-m thick, light-brown layered sequence, characterized by the presence of abundant gypsum crystals (up to 8 cm in maximum size), here-named the Gypsum King sequence (GK sequence). It consists of several fine-grained layers (Figure 3 and 4a), from silty

ACCEPTED MANUSCRIPT

Downloaded from http://sp.lyellcollection.org/ at Universidad Nacional Autonoma De Mexico on August 24, 2021

laminae to silty-sandy centimetric units. At its base, bivalves, 3-5 cm in size were found (Figure 4b). As specimens were extracted from the sediment, they completely disaggregated making it impossible to define their species. Gypsum crystals are also observed from the middle up to the top of the sequence (Figures 4c and d). Sediment samples also show diatom fragments (genus *Aulacoseira*) at microprobe scales (Fig. 4e). The GK sequence is overlain by a younger 4-m thick bright-white lacustrine sequence (Figure 3) with an estimate radiocarbon age of 1815-1992 cal. yrs (Cortés et al., 2010a). This sequence consists of a massive to horizontally stratified fine sand and silty particles, intercalated with slumped horizons, composed mainly of crystals, silica needles, and very common planktonic diatoms. A lahar deposit separates the two sequences. Moving few meters along the terrace wall, the GK deposit increases in thickness up to 4 m where a debris avalanche deposit outcrops at its base. The DAD is matrix-supported, massive, heterogeneous, and poorly sorted with angular to sub-angular fragments showing jigsaw cracks and hydrothermally altered areas (Figure 3).

Detailed investigation of the GK sequence was carried out, including vertical variation in grainsize and chemical composition, which are plotted against the linear age–depth modeling (Table 2, Figure 5). From the bulk-sediments chemical analyses, the S content is included in the diagram, to analyze its possible correlation against eruptive/climatic episodes. Main eruptive events are also identified along the calibrated curve based on Crummy et al. (2019a, b) (Table 1).

Modelled ages show that the sequence spans a period of approximately 1500 yrs. from 8395 to 6492 mean cal. yr (Figures 2 and 5). From the base, the first 40 cm consist of laminae with >90% silt fraction, barren of sand, with an estimated sedimentation rate of 0.15 cm/yr (Figure 5). The bivalve shells yield an age of 8341-8451 cal. yr B.P. (BS sample, table1) in accordance with the ^{14}C of sediment here sampled (C1; see Table 1). At ~ 8189 cal. yr a first S main peak (S1, 0.9 wt %) is identified and gypsum crystals start to appear in the sequence. From this level and up to 7606 cal. yr the sedimentation rate decreases noticeably (LSR = Low Sedimentation Rate), with a main change at *ca.* 8046 (0.05 cm/yr), when a S peak is also detected (S2, 1.22 wt %), and at 7852 cal. yr (0.03 cm/yr), that corresponds to a sudden increase in sand fraction (57 wt %) persisting up to the top of this temporal interval. Based on their ages, the VAC-DAD edifice failure and associated Unit N eruptive activity correlate with the observed increase in grainsize (Figure 5). From 7606 cal. yr the sediment rate increases and maintains a constant trend up to the top of the sequence (0.11 yr/cm). At 7522 cal. yr the largest peak in S is identified (S3, 1.85 wt %), contemporaneous to the initial eruptive phase of Unit O; a secondary increase in S content (S4, ~1 wt %) is observed in correspondence with the final stages of this eruptive period. During this time interval two other

ACCEPTED MANUSCRIPT

Downloaded from http://sp.lyellcollection.org/ at Universidad Nacional Autonoma De Mexico on August 24, 2021

discrete increases in sand fraction are also observed. Gypsum crystals are common in this portion of the section. The last 30 cm of the sequence, which yielded a ^{14}C age of 7308 cal. yr BP (C5), consists of a brown, homogeneous fine silty paleosol, characterized by well-developed mud cracks.

6. Discussion

Lacustrine sediments have been extensively used for paleoclimatic reconstruction (Ortega et al., 2002; Hodell et al., 2008) and, in volcanic environments, as an intact record of past eruptive episodes (Caballero et al., 2001). Usually, the sediments belong to long-lived and still active lakes where several meters of sediments accumulated over thousands of years preserve valuable information on the surrounding environment and its response to climatic and hydrologic changes. Lakes formed by river impoundment due to a gravitational mass collapse in mountain areas have been recognized as a common phenomenon. However, if they lack a natural draining system, their longevity is reduced as the high-water discharge from the river can quickly induce failure of the natural dam (Fan et al., 2020). Due to their short lifespan and small extent, sedimentation in these lakes can be too short-lived and chaotic to preserve evidence of paleoenvironmental changes or, in case of a volcanic environment, the stratigraphic record of fine ash from past eruptions. Only a few cases where the sediments from these short-lived lakes have recorded paleoenvironmental information have been previously reported: for example, the Skagit River in Washington state was dammed by a landslide at 7040 yr B.P, giving rise to Lake Ksnea, this allowed remobilized tephra from the cataclysmic eruption of Mount Mazama at 6730 yr B.P. to be deposited in the lake (Riedel et al., 2001); Intra-hummock lacustrine sediments preserved at Volcán de Colima, yield the first and unique evidence of hydromagmatic activity occurring at 15 cal. kyr BP at this volcano (Roverato et al., 2013); sediments from Chungará lake, formed as a result of impounding of the Lauca River by the partial collapse of Parinacota volcano at 8 kyr BP, were studied to evaluate environmental (volcanic vs. climatic) controls on lacustrine sedimentation in northern Chile (Sáez et al., 2007). The GK sequence represents a rare example of sediments accumulated in a temporary lake in a volcanic environment, providing invaluable data about the Early Holocene eruptive activity of Volcán de Colima and the first evidence of the 8.2 kyr event at this latitude.

6.1 The temporary dam

The GK sequence corresponds to a lacustrine sequence, as supported by the textural features observed, such as cm-thick silty-clay laminated layers, and the presence of bivalves and diatoms. Based on its extent, it represents a hanging sequence suspended in the upper portion of a terrace up to 80 m high along the Los Ganchos ravine, mostly formed by a debris avalanche deposit (Figures

ACCEPTED MANUSCRIPT

Downloaded from http://sp.lyellcollection.org/ at Universidad Nacional Autonoma De Mexico on August 24, 2021

6a). The age of the DAD outcropping at the base of the sequence is unknown but assumptions on its origin and age are possible. Three main debris avalanche deposits have been reported in this sector by Cortés et al. (2010b; 2019), at 25029-26638 cal. yr BP (El Tecuan Debris avalanche, ET-DAD), the 10755-11230 cal. yr BP MY-DAD and the 3594-4242 cal. yr BP LG-DAD (Table 1, Figure 6a). The MY-DAD deposit outcrops on the SW side of the volcano, downstream with respect to the studied lacustrine section (Figure 6a) and represents the youngest collapse event preceding the GK sequence. The ET-DAD outcrops towards the N where it is directly overlaid by the LG-DAD (Cortés et al., 2010a,b), as observed at section LA2 where a paleosol separating these two debris avalanche deposits was here dated at 18644-19013 cal. yr BP (Figure 6a; Table 1). In addition, Cortés et al. (2010a,b) also reported lacustrine sediments along the Huacal ravine (Figure 6a, black triangle), dated at 7924-8481 cal yr BP, also containing gypsum fragments and directly overlying the ET-DAD debris avalanche deposit. Based on these ages, it is likely that emplacement of the MY-DAD obstructed the full width of the Armeria river and collapsed materials distributed both up- and downstream also affected tributary valleys (type IIIa dam, Casagli and Ermini, 1999), forming a main temporary lake along the Armeria valley, as well as small lateral impoundments along the Los Ganchos (Figure 6b) and Huacal ravines. Cortés et al. (2019) mapped a stratigraphic lateral contact between ET-DAD and MY-DAD deposits, based only on the exposures of the basal portion of > 100m-thick terrace along the La Lumbre river (Figure 6a). However, considering the difference in topographic altitude between both terraces (see topographic profiles in Figure 6a), the MY-DAD deposit is 50 m thicker than the ET-DAD, suggesting that MY-DAD was probably able to overflow the older ET-DAD deposit reaching and filling the Armeria river up-valley (white dotted line, Figure 6a). Examples of similar processes causing DAD deposits superposition are common at Volcán de Colima (Komorowski et al., 1997; Cortes et al., 2019). We propose the extent of the temporary lake based on the 680 m a.s.l. topographic contour, representing the altitude at which the lacustrine sequence outcrops along the Los Ganchos ravine. We also suggest that along the Armeria valley part of the DAD was rapidly removed by overtopping, but the smaller and shallower impoundments formed in the obstructed lateral Los Ganchos and Huacal ravines resisted longer as they formed on low discharge/ephemeral drainages (Figure 6b). Importantly, the GK sequence represents only a marginal portion of the entire lacustrine sequence, and the whole lacustrine package is much thicker in different sectors. In this sense, its age does not exactly represent the maximum age of the entire lacustrine sedimentation (i.e. the age of the temporary lake), but because of the inaccessible outcrop conditions (vertical wall), it is impossible to obtain samples from lower sections of the sequence.

6.2. Volcanological and Climatological implications.

ACCEPTED MANUSCRIPT

Downloaded from http://sp.lyellcollection.org/ at Universidad Nacional Autonoma De Mexico on August 24, 2021

Temporary damming of the Los Ganchos ravine formed an endorheic lake which reached its highest level close to the steep slopes of Volcán de Colima at ~8400 cal. yr BP, and accumulated sediments for a period of ~1500 years with extremely low-sedimentation rates (~0.1-0.05 cm/y).

Changes in sedimentation rate and peaks in S content observed along the sediment column can be either correlated with the change in climatic condition or with the eruptive activity of Volcán de Colima. Sulfur ions in oxidized terrestrial freshwater are usually found as SO_4^{2-}, and reflects the eroded and soluble fraction from rocks, soils and minerals from the local region. Although the sulfur cycle in lakes and lake sediments is complex (Holmer and Storkholm, 2001), the variability in S concentration is usually interpreted as a proxy of dry conditions, as a reduction in lake volume due to evaporation exceeding precipitation can lead to gypsum saturation and precipitation (e.g. Hodell et al., 2008). On the other hand, volcanic activity can also contribute to the sulfur concentration in lake sediments due to the atmospheric deposition of SO_2 aerosols. Indeed, SO_2 concentration within a volcanic plume is several orders of magnitude greater than in ambient air, and its plume concentration is usually proportional to the magnitude of the eruption (Oppenheimer, 2003; Pfeffer et al., 2006; Carn et al., 2016). SO_2 is transported away from the volcanoes until it is oxidized to SO_4^{2-} which can reach the surface by, either dry or wet deposition. The former implies the incorporation of sulfate at the surface of particulates which are deposited on the ground, whilst wet deposition includes removal of sulfate particles by rainfall. The SO_2 average residence time in the atmosphere is ~25 hours, but it can be as large as 60 – 100 h depending on the removal mechanism (Seinfeld and Pandis, 2006). In this light, we interpret the S variability in the GK stratigraphic column to reflect changes in the hydrological balance of the dammed Armeria river, with SO_2/SO_4^{2-} inputs from volcanic aerosols emitted during the contemporaneous activity of Volcán de Colima

Figure 5 shows that, between 8189 and 8046 cal. yrs, a significant increase in sulfur concentration (S1 and S2 peaks) corresponds to a phase of apparent volcano quiescence, when a decrease in sedimentation rate is also detected. We interpret these excursions to represent a phase of low lake level and low sedimentation as a result of a suppressed North American monsoon during the 8.2 kyr event. These peaks are consistent with the structure and chronology of the 8.2 kyr event observed in Greenland Ice-cores (Thomas et al 2007), and, importantly with multiple speleothem $\delta^{18}O$ records from Brazil, Oman, and China that record the effect of proglacial lake outburst floods on North Atlantic ocean circulation patterns on the different monsoonal systems (Cheng et al., 2009). We note that a suppressed monsoon during the 8.2 kyr event is consistent with previous observations in Central America (Lachniet et al 2004a) and southwestern Mexico (Bernal et al 2011). with dry conditions in Zirahuen, Michoacán, (Lozano-García et al., 2013) and at Iztaccíhuatl volcano,

ACCEPTED MANUSCRIPT

Downloaded from http://sp.lyellcollection.org/ at Universidad Nacional Autonoma De Mexico on August 24, 2021

where temporary expansion of the glacier was also contemporaneous to the event (Lozano-García and Vázquez-Selem, 2005). Furthermore, modelling data suggest that the abrupt incursion of cold and freshwater into the North Atlantic, results in a southward migration of the ITCZ (LeGrande and Schmidt, 2008; Broccoli et al., 2006). Our interpretation of a suppressed North American monsoon does not imply a total collapse of the monsoonal system, as sedimentation was maintained throughout the duration of the event and no hiatuses were detected. Rather, our results suggest that during the event, evapotranspiration at the lake was higher, probably due to lower rainfall and a more intense or longer dry season, leading to lower lake levels and even seasonal lakebed exposure, hence, gypsum precipitation.

After the conclusion of the North Atlantic event at ~8050 yr B.P. (Thomas et al., 2007), the North American monsoon was restored, albeit at a level somewhat less intense than prior to the 8.2 kyr event as attested by the $\delta^{18}O$ data from Cueva del Diablo (Bernal et al., 2011). However, the record analyzed here still shows a decrease in sedimentation rate and an increase in sediment grainsize. These changes are correlated with the 7590-8172 cal. yr edifice collapse and the emplacement of the related 16 km^3 VAC-DAD (Cortés et al., 2019) towards the south. This volcanic event, correlated with the massive tephra fall deposits of Unit N (Crummy et al., 2019b) (Figure 5), likely modified regional hydrologic networks significantly, and increased sediment availability on the volcano slopes. Sedimentation continued for approximately 700 years, partially recovering the hydrological network and the sedimentation rate to levels similar to those prior to the 8.2 kyr event. During this period an intense eruptive phase has been identified (Unit O) with the emplacement of a thick sequence (from 30 cm to more than 100 cm) of ash falls and surges separated by multiple gaps of ~ 100 years (Crummy et al., 2019a). A clear eruptive reconstruction of this eruptive phase has not been previously described due to its poorly exposure, but the younger S3 and S4 peaks can be here used to identify the main eruptive episodes during the emplacement of Unit O (Figure 5). Importantly, since the fall deposits from these eruptions were dispersed towards the northeastern of Volcán de Colima (Crummy et al., 2019a,b), a record of such an event in the GK sequence was unexpected. However, our results indicate that, despite ash-plume dispersal towards the NE, sulfate aerosols were deposited along the Los Ganchos dammed ravine, as recorded by the GK sequence (Figure 6). Moreover, because of the short residence time of SO_2 aerosols in the atmosphere, our results allow us to constrain the age of the main eruptions episodes belonging to Unit O to the age of the S3 and S4 peaks in our age model: i.e. to 7404-7723 and 6984-7330 yr BP (2sigma), respectively (Table 2).

ACCEPTED MANUSCRIPT

Downloaded from http://sp.lyellcollection.org/ at Universidad Nacional Autonoma De Mexico on August 24, 2021

The final demise of the lake probably occurred by progressive evaporation as indicated by the presence of gypsum crystals in the upper part of the sequence that remained exposed for sufficient time for the formation of a soil with well-developed mud cracks. Exposure of the uppermost sediments eventually led to pedogenesis, which continued until renewed damming of the Ganchos River at 3600 yr B.P. and the resumption of lacustrine sedimentation (Cortés et al., 2010a).

7. Conclusion

The GK lacustrine sequence is an interesting and new record of the Early Holocene eruptive history of the Volcán de Colima, and provides the first evidence of consequences of the 8.2 kyr global climate event on the North American monsoon in this region marked by significant sulfur peaks coinciding with decreases in sedimentation rates between 8189 and 2046 cal. years. This record is particularly relevant considering the lake was transiently formed as a secondary effect from the catastrophic destruction of a volcanic edifice. Despite its short lifespan, and the low sampling resolution, it was possible to record environmental variations at both local and global scales. Total S content was here used to identify the signature of the main eruptions of Volcán de Colima during Early Holocene, an unexpected result considering that the lake was located upwind from the main dispersal axis of the eruptive columns. Moreover, our results suggest that even if the deposition of volcanic ash is modulated by wind direction, deposition (dry and/or wet) of SO_2 aerosols can occur radially around the main volcanic edifice, especially at low altitudes where wind directions can be highly variable. Even if the isotopic composition of S should be measured to better discriminate its source, the results obtained here point to the possibility of exploring lacustrine sediments in other volcanic environments with a different perspective, which usually only look for fine ash layers intercalated in the lacustrine sequences.

Acknowledgements

We thank Marina Vega Gonzalez for SEM analysis. The authors would like to thank Rufino Lozano Santa-Cruz, Lucy Mora-Palomino and Kumiko Shimada from LANGEM-Instituto de Geología – UNAM for their technical support and geochemical analyses. We are grateful to reviewers Julia Crummy and Vern Manville for their accurate corrections, comments and suggestions.

ACCEPTED MANUSCRIPT

Downloaded from http://sp.lyellcollection.org/ at Universidad Nacional Autonoma De Mexico on August 24, 2021

Author contributions

LC, JPB, MR: conceptualization, data curation, methodology, writing – review and editing; **AC**: conceptualization (supporting), investigation (supporting).

Funding information

This work was supported by projects CONACyT 220786 to L. Capra and DGAPA-UNAM IN108419 to J.P. Bernal.

References

Alley, R.B., Ágústsdóttir, A.M. 2005. The 8k event: Cause and consequences of a major Holocene abrupt climate change. *Quaternary Science Reviews,* **24**, 1123–1149.

Alley, R.B., Mayewski, P.A., Sowers, T., Stuiver, M., Taylor, K.C., Clark, P.U. 1997. Holocene climatic instability: A prominent, widespread event 8200 yr ago. *Geology,* **25**, 483–486.

Barber, D.C., Dyke, A., Hillaire-Marcel, C., Jennings, A.E., Andrews, J.T., Kerwin, M.W., Bilodeau, G., McNeely, R., Southon, J., Morehead, M.D., Gagnon, J.-M. 1999. Forcing of the cold event of 8,200 years ago by catastrophic drainage of Laurentide lakes. *Nature,* **400**, 344–348.

Bernal, J.P., Lachniet, M., McCulloch, M., Mortimer, G., Morales, P., Cienfuegos, E. 2011. A speleothem record of Holocene climate variability from southwestern Mexico. *Quaternary Research*, **75**, 104–113.

Blaauw, M. and Christen, J.A. 2011. Flexible paleoclimate age-depth models using an autoregressive gamma process. *Bayesian Analysis*, **6(3)**, 457-474.

Broccoli, A.J., Dahl, K.A., Stouffer, R.J. 2006. Response of the ITCZ to Northern Hemisphere cooling. *Geophysical Research Letters*, **33**, L01702.

Caballero, M., Macías, J. L., Lozano-García, S., Urrutia-Fucugauchi, J., Castañeda-Bernal, R. 2001. Late Pleistocene –Holocene volcanic stratigraphy and palaeoenvironments of the upper Lerma basin, Mexico. *In*: White, J.D.L. and Nancy R. Riggs, N.R. (eds) *Volcaniclastic Sedimentation in Lacustrine Settings*. Blackwell Science Ltd, 247–261, doi:10.1002/9781444304251.

Caballero, M., Vilaclara, G., Rodríguez, A., & Juárez, D. 2003. Short-term climatic change in lake sediments from lake Alchichica, Oriental, Mexico. *Geofísica Internacional*, ***42*(3)**, 529-537.

Capra, L., 2007. Volcanic natural dams: identification, stability, and secondary effects. *Natural Hazards*, **43**, 45-61.

Capra, L. and Macías, J.L. 2002. The cohesive Naranjo debris flow deposit (10 km3): a dam breakout flow derived from the Pleistocene debris-avalanche deposit of Nevado de Colima volcano (México). *Journal of Volcanology and Geothermal Research*, **117**, 213–235.

Capra, L., Macías, J.L., Cortés, A., Dávila, N., Saucedo, R., Osorio-Ocampo, S., Arce, J.L., Gavilanes-Ruiz, J.C., Corona-Chávez, P., García-Sánchez, L., Sosa-Ceballos, G., Vázquez, R. 2015. Preliminary report on the July 10–11, 2015 eruption at Volcán de Colima: Pyroclastic density currents with exceptional runouts and volume. *Journal of Volcanology and Geothermal Research*, **310**, 39-49.

Carn, S.A., Clarisse, L., Prata, A.J. 2016. Multi-decadal satellite measurements of global volcanic degassing. *Journal of Volcanology and Geothermal Research*, **311**, 99–134.

Casagli, N. and Ermini, L. 1999. Geomorphic analysis of landslide dams in the Northern Apennine. *Trans. Jpn. Geomorphol.,* **20 (3)**, 219–249.

Cheng, H., Fleitmann, D., Edwards, L.R., Wang, X., Cruz, F.W., Auler, A.S., Mangini, A., Wang, Y., Kong, X., Burns, S.J., Matter, A. 2009. Timing and structure of the 8.2 kyr B.P. event inferred from $\delta^{18}O$ records of stalagmites from China, Oman, and Brazil. *Geology*, **37**, 1007-1010.

Clarke, G., Leverington, D., Teller, J., Dyke, A. 2003. Superlakes, Megafloods, and Abrupt Climate Change. *Science*, **301**, 922-923.

Cortés, A., Macías, J.L., Capra, L., Garduño-Monroy, V.H. 2010a. Sector collapse of the SW flank of Volcán de Colima, México. The 3600 yr BP La Lumbre-Los Ganchos debris avalanche and associated debris flows. *Journal of Volcanology and Geothermal Research*, **197**, 52–66.

Cortés, A., Garduño, V.H., Macías, J.L., Navarro-Ochoa, C., Komorowski, J.C., Saucedo, R., Gavilanes,

ACCEPTED MANUSCRIPT

Downloaded from http://sp.lyellcollection.org/ at Universidad Nacional Autonoma De Mexico on August 24, 2021

J.J. 2010b. Geologic mapping of the Colima volcanic complex (Mexico) and implications for hazard assessment. *In*: Groppelli, G. and Viereck-Goette, L. (eds) Stratigraphy and Geology of Volcanic Areas. *Geological Sociaty of America, special papers,* **464**, 249-264, DOI: 10.1130/2010.2464(12).

Cortés, A., Komorowski, J-C, Macias, J.L., Capra, L., Layer, P. 2019. Late Pleistocene-Holocene debris avalanche deposits from Volcán de Colima, México. *In*: Varley, N., Komorowski, J.C., Connor, C. (eds) *Volcán de Colima: Portrait of a persistently hazardous volcano. Active volcanoes of the world series.* Springer, 55-88.

Costa, J.E. and Schuster, R.L., 1988. The formation and failure of natural dams. *Geological Society of America Bulletin*, **100**, 1054-1068.

Costa, J.E., Schuster, R.L. 1991. Documented historical landslide dams from around the world. *USGS Open-File Report,* **91-239**, 44pp.

Crummy, J.M., Savov, I.P., Navarro-Ochoa, C., Morgan, D.J. 2019a. Holocene eruption history and magmatic evolution of the Colima volcanic complex. *In*: Varley, N., Komorowski, J.C., Connor, C. (eds) *Volcán de Colima: Portrait of a persistently hazardous volcano. Active volcanoes of the world series.* Springer, 1-25.

Crummy, J.M., Savov, I.P., Loughlin, S.C., Connor, C.B., Connor, L., Navarro-Ochoa, C. 2019b. Challenges of determining frequency and magnitudes of explosive eruptions even with an unprecedented stratigraphy. *Journal of Applied Volcanology,* **8,**3.

Davila, N., Capra, L., Ferrés, D., Gavilanes-Ruiz, J.C., Flores, P. 2019. Chronology of the 2014–2016 Eruptive Phase of Volcán de Colima and Volume Estimation of Associated Lava Flows and Pyroclastic Flows Based on Optical Multi-Sensors. *Remote Sensing*., **11**, 1167.

Dixit, Y., Hodell, D.A., Sinha, R., Petrie, C.A. 2014. Abrupt weakening of the Indian summer monsoon at 8.2 kyr B.P. *Earth and Planetary Science Letters*, **391,** 16-23.

Elison, C.R.W., Chapman, M.R., Hall, I.R. 2006. Surface and Deep Ocean Interactions During the Cold Climate Event 8200 Years Ago. *Science*, **312**, 1929-1932.

Fan, X., Dufresne, A., Subramanian, S., Strom, A., Hermanns, R., Stefanelli, C., Hewitt, K., Yunus, A., Dunning, S., Capra, L., Geertsema, M., Miller, B., Casagli, N., Jansen, J., Xu, Q. 2020. The formation and impact of landslide dams – State of the art. *Earth-Science Reviews*, **203**, 103116.

Heard, K., Turney, C.S.M., Pilcher, J.R., Palmer, J.G., Baillie, M.G.L. 2007. Problems with identifying the 8200-year cold event in terrestrial records of the Atlantic seaboard: a case study from Dooagh, Achil Island, Ireland. *Journal of Quaternary Science,* **22**, 65-75.

Hodell, D.A., Anselmetti, F.S., Ariztegui, D., Brenner, M., Curtis, J.H., Gilli, A., Grzesik, D.A., Guilderson, T.J., Muller, A.D., Bush, M.B., Correa-Metrio, A., Escobar, J., Kutterolf, S., 2008. An 85-ka record of climate change in lowland Central America. *Quaternary Science Reviews*, **27(11-12),** 1152-1165.

Holmer, M. and Storkholm, P. 2001. Sulphate reduction and sulphur cycling in lake sediments: a review. *Freshwater Biology*, **46(4)**,431-451.

Hughen, K.A., Overpeck, J.T., Lehman, S.J., Kashgarian, M., Southon, J., Peterson, L.C,. Alley, R., Sigman, D.M. 1998. Deglacial changes in ocean circulation from an extended radiocarbon calibration. *Nature*, **391**, 65-8.

Komorowski, J.C., Navarro, C., Cortes, A., Saucedo, R., Gavilanes, J.C., Siebe, C., Espíndola, J.M., Rodriguez-Elizarrarás, S.R. 1997. The Colima Volcanic Complex, Field guide #3, IAVCEI. General Assembly, Puerto Vallarta, Mexico.

Lachniet, M.S., Asmerom, Y., Burns, S.J., Patterson, W.P., Polyak, V.J., Seltzer, G.O. 2004a. Tropical response to the 8200 yr BP cold event? Speleothem isotopes indicate a weakened early Holocene monsoon in Costa Rica. *Geology*, **32**, 957-960.

Lachniet, M., Burns, S.J., Piperno, D.R., Asmerom, Y., Polyak, V.J., Moy, C.M., Christenson, K. 2004b. A 1500-year El Niño/Southern Oscillation and rainfall history for the Isthmus of Panama from speleothem calcite. *Journal of Geophysical Research*, **109**, D20117.

LeGrande, A.N., Schmidt, G.A., Shindell, D.T., Field, C.V., Miller, R.L., Koch, D.M., Faluvegi, G., Hoffmann, G. 2006. Consistent simulations of multiple proxy responses to an abrupt climate

ACCEPTED MANUSCRIPT

Downloaded from http://sp.lyellcollection.org/ at Universidad Nacional Autonoma De Mexico on August 24, 2021

change event. *Proceedings of the National Academy of Sciences of the United States of America,* **103**, 837-842.

LeGrande, A.N. and Schmidt, G.A. 2008. Ensemble, water isotope–enabled, coupled general circulation modeling insights into the 8.2 ka event. *Paleoceanography*, **23(3)**, PA3207.

Lozano, R. and Bernal, J.P. 2005. Characterization of a new set of eight geochemical reference materials for XRF major and trace element analysis. *Revista Mexicana de Ciencias Geológicas*, **22(3)**, 329-344.

Lozano-García, M.S. and Vázquez-Selem, L. 2005. A high elevation Holocene pollen record from Iztaccihuatl volcano, Central México. *The Holocene*, **15 (3)**, 329-338.

Lozano-García, M.S., Torres-Rodriguez, E., Ortega, B., Vázquez, G., Caballero, M. 2013. Ecosystem responses to climate and disturbances in western central Mexico during the late Pleistocene and Holocene. *Palaeogeography, Palaeoclimatology, Palaeoecology,* **370**, 184-195.

Luhr, J.F., Navarro-Ochoa, C., Savov, I.P. 2010. Tephrochronology, petrology and geochemistry of Late-Holocene pyroclastic deposits from Volcán de Colima, Mexico. *Journal of Volcanolology and Geothermal Research*, **197**,1–32.

Macías, J.L., Saucedo, R., Gavilanes, J.C., Varley, N., Velasco García, S., Bursik, M.I., Vargas Gutiérrez, V., Cortes, A. 2006. Flujos piroclásticos asociados a la actividad explosiva del volcán de Colima y perspectivas futuras. *GEOS*, **25 (3)**, 340–351.

Macorps, E. Charbonnier, S.J., Varley, N.R., Capra, L., Atlas, Z., Cabré, J. 2018. Stratigraphy, sedimentology and inferred flow dynamics from the July 2015 block-and-ash flow deposits at Volcán de Colima, Mexico. *Journal of Volcanology Geothermal Research*, **349**, 99–116.

Mingram, J., Allenb, J.R.M., Br.uchmanna, C., Liuc, J., Luoc, X., Negendanka, J.F.W., Nowaczyka, N., Schettlera, G. 2004. Maar- and crater lakes of the Long Gang Volcanic Field (N.E. China) - overview, laminated sediments, and vegetation history of the last 900 years. *Quaternary International*, **123–125**, 135–147.

Morrill, C., LeGrande, A.N., Renssen, H., Bakker, P., Otto-Bliesner, B.L. 2013. Model sensitivity to North Atlantic freshwater forcing at 8.2 ka. *Climate of the Past,* **9**, 955-968.

Oppenheimer, C. 2003. Climatic, environmental and human consequences of the largest known historic eruption: Tambora volcano (Indonesia) 1815. *Progress in Physical Geography*, **27 (2)**, 230-259.

Ortega, B., Caballero, C., Lozano, S., Israde, I., Vilaclara, G. 2002. 52 000 years of environmental history in Zacapu basin, Michoacan, Mexico: the magnetic record. *Earth and Planetary Science Letters*, **202(3-4)**, 663-675.

Pfeffer, M., Langmann, B., Graf, H. 2006. Atmospheric transport and deposition of Indonesian volcanic emissions. *Atmospheric Chemistry and Physics*, **6(9)**, 2525-2537.

Reimer, P., Austin, W., Bard, E., Bayliss, A., Blackwell, P., Bronk Ramsey, C. et al. 2020. The IntCal20 Northern Hemisphere Radiocarbon Age Calibration Curve (0–55 cal kBP). *Radiocarbon*, **62(4)**, 725-757. doi:10.1017/RDC.2020.41

Riedel, J.L., Pringle, P.T. and Schuster, R.L. 2001. Deposition of Mount Mazama Tephra in a Landslide-Dammed Lake on the Upper Skagit River, Washington, USA. *In*: White, J.D.L. and Nancy R. Riggs, N.R. (eds) *Volcaniclastic Sedimentation in Lacustrine Settings*. Blackwell Science Ltd, 285-298, doi:10.1002/9781444304251.

Roverato, M., Capra, L., Sulpizio, R., Norini, G. 2011. Stratigraphic reconstruction of two debris avalanche deposits at Colima Volcano (Mexico): insights into pre-failure conditions and climate influence. *Journal of Volcanology and Geothermal Research,* **207**, 33–46.

Roverato, M., and Capra, L. 2013, Características microtexturales como indicadores del transporte y emplazamiento de dos depósitos de avalancha de escombros del volcán de Colima. *Revista Mexicana de Ciencias Geológicas*, **30**, 512–525.

Roverato M., Capra L., Sulpizio R. 2013. First evidence of hydromagmatism at Colima volcano (Mexico). *Journal of Volcanology and Geothermal Research*, **249**, 197–200.

Sáez, A., Valero-Garces, B., Moreno, A., Bao, R., Pueyo, J., Gonzalez-Samperiz, P., Giralt, S., Taberner,

ACCEPTED MANUSCRIPT

Downloaded from http://sp.lyellcollection.org/ at Universidad Nacional Autonoma De Mexico on August 24, 2021

C., Herrera, C., Ibert, R. 2007. Lacustrine sedimentation in active volcanic settings: the Late Quaternary depositional evolution of Lake Chungará (northern Chile). *Sedimentology*, **54(5)**, 1191-1222.

Seinfeld, J. H. and Pandis, S. N. (eds) 2006. *Atmospheric Chemistry and Physics: From Air Pollution to Climate Change.* John Wiley & Sons, Inc., 1152.

Stuiver, M., Reimer, P.J., and Reimer, R.W. 2021. CALIB 8.2 [WWW program] at http://calib.org, accessed 2021-3-29.

Thomas, E.R., Wolff, E.W., Mulvaney, R., Steffensen, J.P., Johnsen, S.J., Arrowsmith, C., White, J.W.C., Vaughn, B., Popp, T. 2007. The 8.2 ky event from Greenland ice cores. *Quaternary Science Reviews*, **26**, 70–81.

Tibaldi, A., Lagmay, A.M.F., Ponomareva, V.V. 2005. Articles effects of basement structural and stratigraphic heritages on volcano behaviour and implications for human activities (the UNESCO / IUGS / IGCP Project 455). *Episodes*, **28 (3),** 158-70

Vázquez-Selem, L. and Heine, K. 2012. Late Quaternary glaciation in Mexico. *In*: Ehlers, J., Gibbard, P.L., Hughes, P.D. (eds.) *Quaternary Glaciations-Extent and Chronology. A closer look*. Developments in Quaternary Science, Elsevier, 15, 849-861.

Zolitschka, B., Schäbitz, F., Lücke, A., Corbella, H., Ercolano, B., Fey, M., Haberzettl, T., Janssen, S., Maidana, N., Mayr, C., Ohlendorf, C., Oliva, G., Paez, M.M., Schleser, G., Soto, J., Tiberi, P., Wille, M. 2006. Crater lakes of the Pali Aike Volcanic Field as key sites for paleoclimatic and paleoecological reconstructions in southern Patagonia, Argentina. *Journal of South American Earth Science*, **21**, 294–309.

ACCEPTED MANUSCRIPT

Downloaded from http://sp.lyellcollection.org/ at Universidad Nacional Autonoma De Mexico on August 24, 2021

Figure Captions

Figure 1. a) Sketch map of southern North America, Central America and northern South America showing the Trans-Mexican Volcanic Belt (TMVB), the location of Volcán de Colima and the sites where the 8.2 kyr event has been recognized in Mexico, and other locations of climatic proxies; 1) Zirahuen lake (Lozano et al., 2013); 2) El Diablo cave (Bernal et al., 2011); 3) Iztaccíhuatl volcano (Lozano-García and Vázquez-Selem, 2005; 4) Chinchankanab lake (Hodel et al., 1995); 5) Stalagmite V1 (Lachniet et al., 2004a) 6) Cariaco basin (Hughen et al., 1998) ; 7) Tigre Perdido cave (Riechekmann et al., 2012). b) Simplified regional tectonic map depicting the Colima Graben along which main rivers drain to the Pacific coast; Red area refers to the extension of main volcaniclastic sequences associated to the Colima Volcanic Complex activity. VC=Volcán de Colima, NC=Nevado de Colima Volcano, CA=Cantaro Volcano. c) Aster image showing the studied area, the location of the lacustrine stratigraphic section shown in figure 2 (LA1, white triangle) and some lakes that formed after the emplacement of debris avalanche deposits (white dots).

Figure 2. Age-depth model for the GK sequence obtained using Bacon (Blaauw and Christen, 2011). All uncertainties correspond to 2-sigma. Ages were calibrated using the IntCal20 Northern Hemisphere radiocarbon age calibration curve (Reimer et a., 2020). The grey-black area indicates the density of possible solutions for the age model (darker indicate more likely). Red-dotted and black-dotted lines are the most likely solution and its 95% confidence interval, respectively.

Figure 3. a) Schematic stratigraphic sketch of the outcrop at section LA1. B) Panoramic view of the LA1 site and detailed stratigraphic section showing the vertical sequence of layers of the Gypsum King section, showing the presence of bivalves.

Figure 4. a) Picture showing the 180 cm-thick GK sequence sampled at ~ 5-cm interval; b) detail of bivalves encountered at the base of the sequence; c) gypsum crystals dispersed in the fine-laminated layers; d) cm-sized gypsum-crystal; e) diatoms observed by SEM.

Figure 5. Comparison of the sulfur concentration and grain-size results from the GK sequence with other climatic records and contemporaneous eruptions from Volcán de Colima. From top to bottom: A) Greenland composite ice-core $\delta^{18}O$ record from Thomas et. al (2007) showing the double-dip in global temperature during the 8.2 ky event. B) calcite $\delta^{18}O$ record from stalagmite PAD07 from Padre Cave, Brazil, illustrating the intensification of the South American monsoon during the 8.2 ky event, as an example of the global effect that the event had upon monsoonal systems (Cheng et al 2009), C) $\%SO_3$ in the GK sequence, labels show important increases in concentration and are discussed in the text. D) granulometry of the GK sequence. E) age-depth model for the GK sequence cross-referenced with stratigraphy (left) and important eruptions from Volcan de Colima, as summarized by Crummy et al. (2019a). Light-yellow box highlights the 8.2 kyr event. Light-pink box shows the area where a low-sedimentation rate (LSR) is observed in the GK sequence.

Figure 6. a) Distribution of debris avalanche deposits in the studied area. Blue dashed line represents the possible extent of the temporary lake impounded by emplacement of the MY-DAD (10755-11230 cal. yr) along the Armeria River. White dashed line represents the limit of the MY-DAD as inferred in the present work. Topographic profiles show the difference in height of the terraces limiting the La Lumbre river. B) Cartoon explaining the formation of temporary lakes along the Los Ganchos ravine.

ACCEPTED MANUSCRIPT

Downloaded from http://sp.lyellcollection.org/ at Universidad Nacional Autonoma De Mexico on August 24, 2021

Table Captions

Table 1. C14 age of the bivalve and lacustrine sediments from the GK sequences and related deposits

Table 2. Modeled ages, grainsize and Sulfur content of sampled layers.

ACCEPTED MANUSCRIPT

lab code	layer/deposit	C14 age BP	2σ calibrated age (BP)	material	ref
BETA-431812	C5	6380 +/- 40 BP	7251-7364	sediments	1
BETA-431811	C4	6260 +/- 30 BP	7156-7262	sediments	1
BETA-431810	C3	6640 +/- 40 BP	7461-7577	sediments	1
BETA-435219	C2	7500 +/- 30 BP	8284-8382	sediments	1
BETA-435218	C1	7600 +/- 30 BP	8360-8430	sediments	1
BETA-324064	BS	7590 +/-40	8341-8451	bivalve shell	1
BETA-319378	LA2	15710 +/- 70	18644-19013	paleosol	1
	Huacal	7380+/-160	7924-8481	sediments	2
	ET-DAD 21 ky	21545+/-265	25029-26638	organic material	2
	MY-DAD 9.6 ky	9672 +/- 80	10755-11230	organic material	2
	VAC-DAD 7 ky	7040 +/-160	7590-8172	organic material	2
	LG-DAD 3.6 ky	3600+/-120	3594-4242	organic material	2
	ERA-DAD 2.5 ky	2505+/-45	2425-2740	charcoal	2
	Unit O	6200+/-40	7171-6981	charcoal	3
	Unit O	6870+/-60	7587-7800	charcoal	3
	Unit N	7070+/-60	7779-8013	charcoal	3
	Unit M	7120+/-80	7776-8043	charcoal	3
	Unit L	7520+/-50	8280-8402	charcoal	3

4C analyses were performed at BETA Laboratory. Radiocarbon dates were calibrated with the program CALIB 8.2 (Stuiver et al., 2021) based on the IntCal20 Northern Hemisphere radiocarbon age calibration curve (Reimer et a., 2020). References : 1 this work; 2 Cortes et al., 2005; 3. Crummy et al., 2019.

ACCEPTED MANUSCRIPT

Table 1

	cal yr BP				*granisize (wt%)*			
depth (cm)	**min**	**max**	**median**	**mean**	**sand**	**silt**	**clay**	**SO3 (wt%)**
3	6492	7003	6792	6778	0.05	92.46	7.47	0.45
18	6702	7132	6941	6933	0.32	92.30	7.38	0.19
28	6873	7209	7035	7036	0.09	92.25	7.66	0.34
39	6984	7284	7112	7114	0.15	89.94	9.89	0.96
47	7061	7330	7168	7171	0.02	85.45	14.54	0.87
56	7161	7394	7234	7237	20.65	74.19	5.15	0.37
59	7177	7416	7257	7261	4.31	90.92	4.77	0.37
69	7241	7515	7340	7349	37.85	58.45	3.73	0.70
76	7290	7584	7400	7408	1.21	91.90	6.92	1.21
89	7404	7723	7510	7522	0.04	92.34	7.60	1.85
97	7505	7814	7585	7606	53.81	43.29	2.91	1.04
106	7717	7969	7854	7852	57.44	39.96	2.62	0.18
116	7912	8165	8049	8048	0.07	90.26	9.69	1.22
120	7974	8215	8116	8106	0.02	89.15	10.81	0.52
129	8059	8290	8213	8189	0.00	91.59	8.38	0.90
143	8155	8373	8288	8279	0.10	91.21	8.76	0.27
155	8271	8439	8357	8355	0.02	93.80	6.19	0.39
165	8350	8503	8409	8414	0.17	91.71	8.14	0.34
173	8395	8589	8455	8469	0.03	91.95	8.02	0.53

ACCEPTED MANUSCRIPT

Table 2

Downloaded from http://sp.lyellcollection.org/ at Universidad Nacional Autonoma De Mexico on August 24, 2021

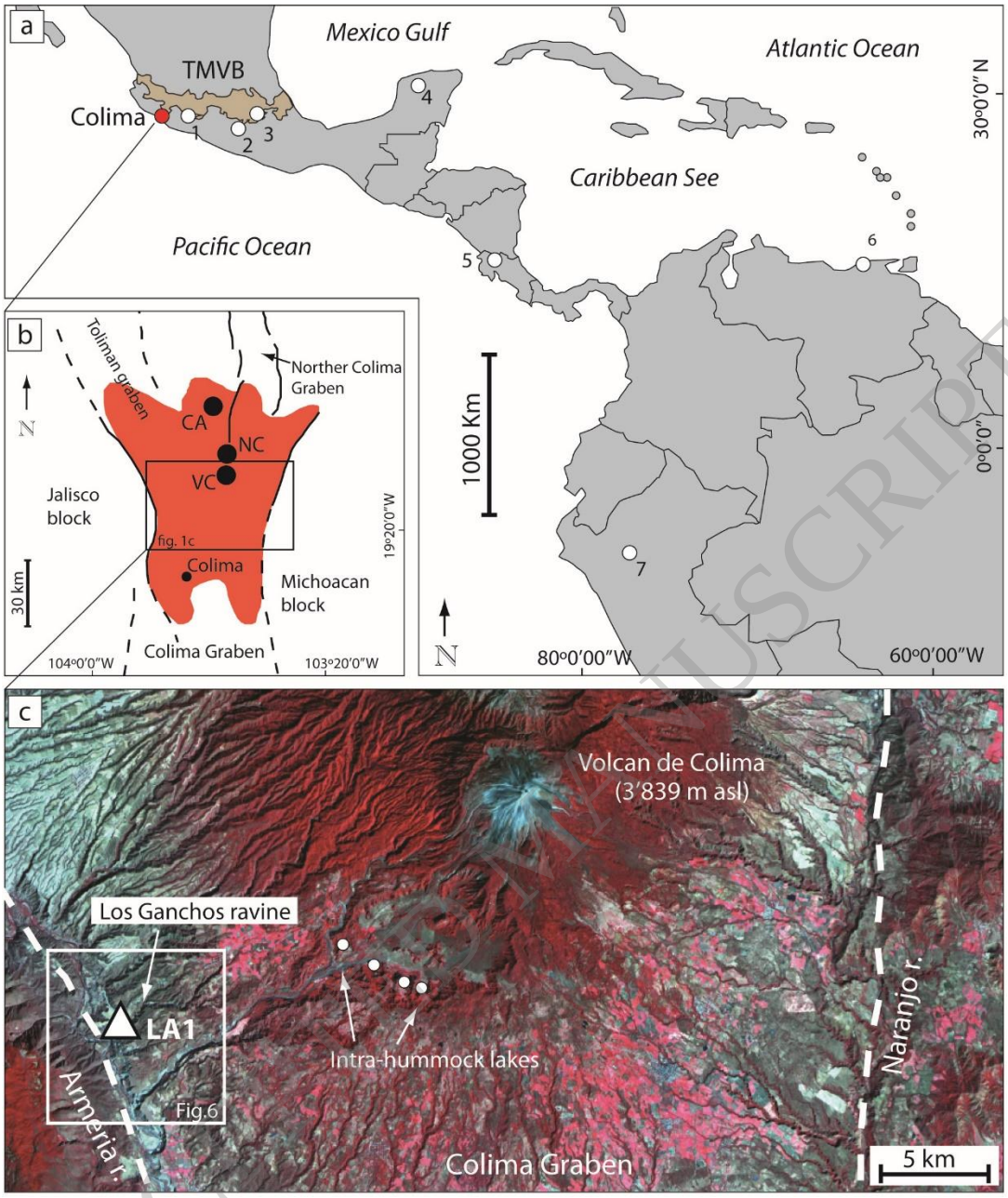

Figure 1

ACCEPTED MANUSCRIPT

Downloaded from http://sp.lyellcollection.org/ at Universidad Nacional Autonoma De Mexico on August 24, 2021

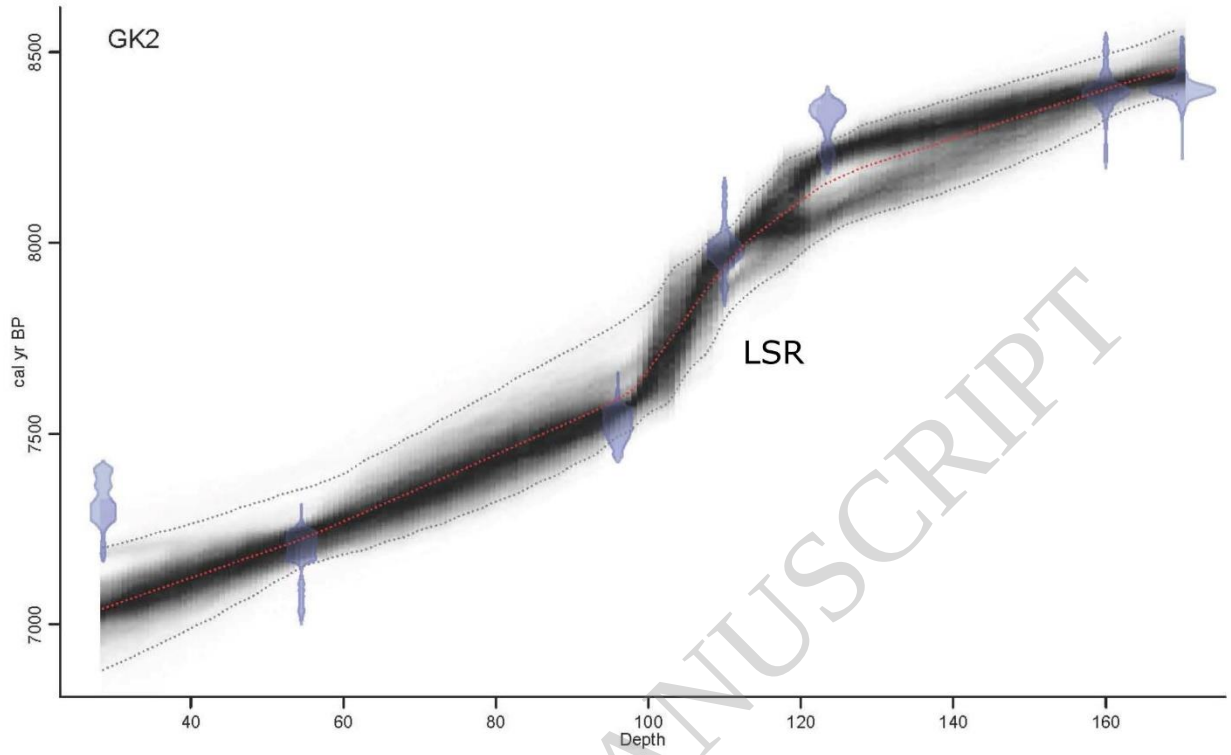

ACCEPTED MANUSCRIPT

Figure 2

Downloaded from http://sp.lyellcollection.org/ at Universidad Nacional Autonoma De Mexico on August 24, 2021

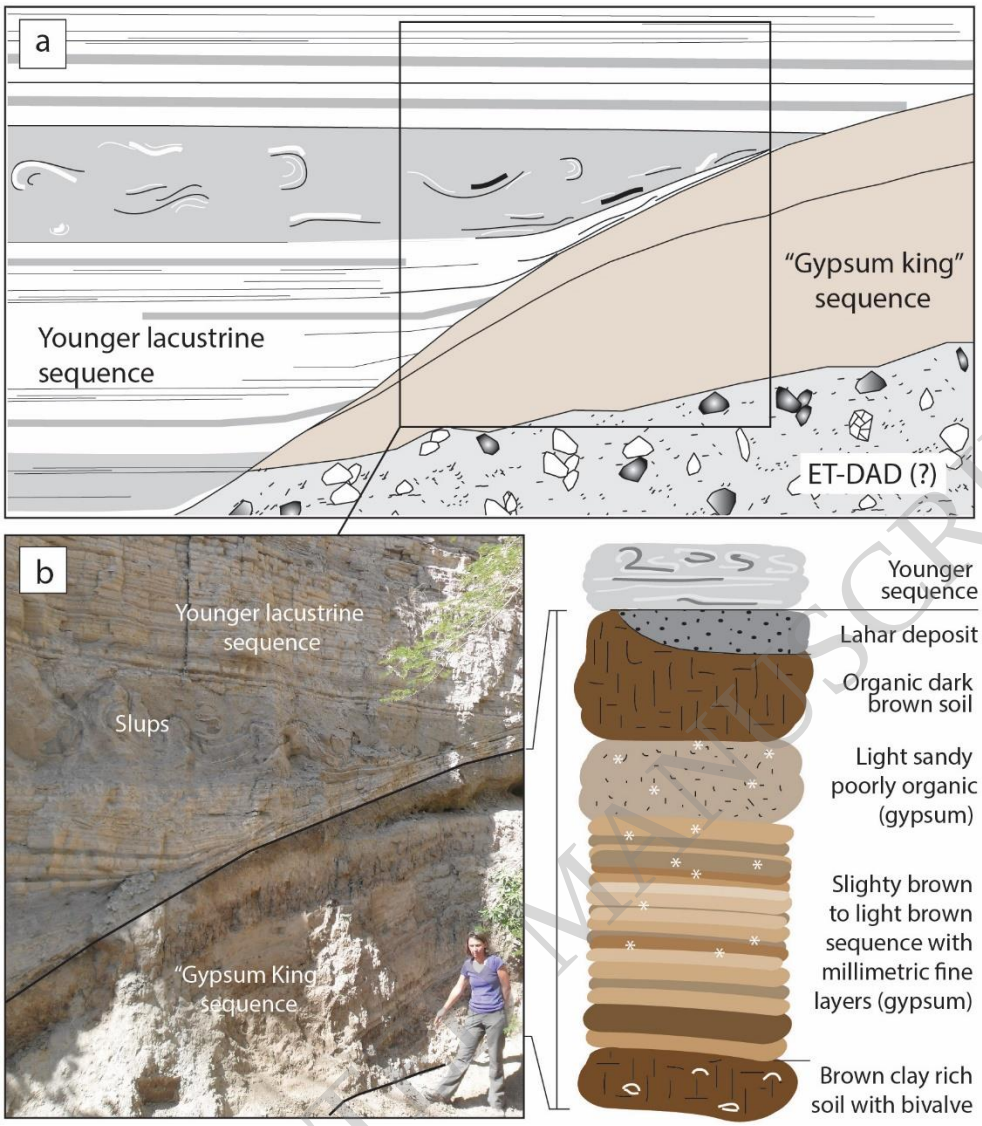

ACCEPTED MANUSCRIPT

Figure 3

Downloaded from http://sp.lyellcollection.org/ at Universidad Nacional Autonoma De Mexico on August 24, 2021

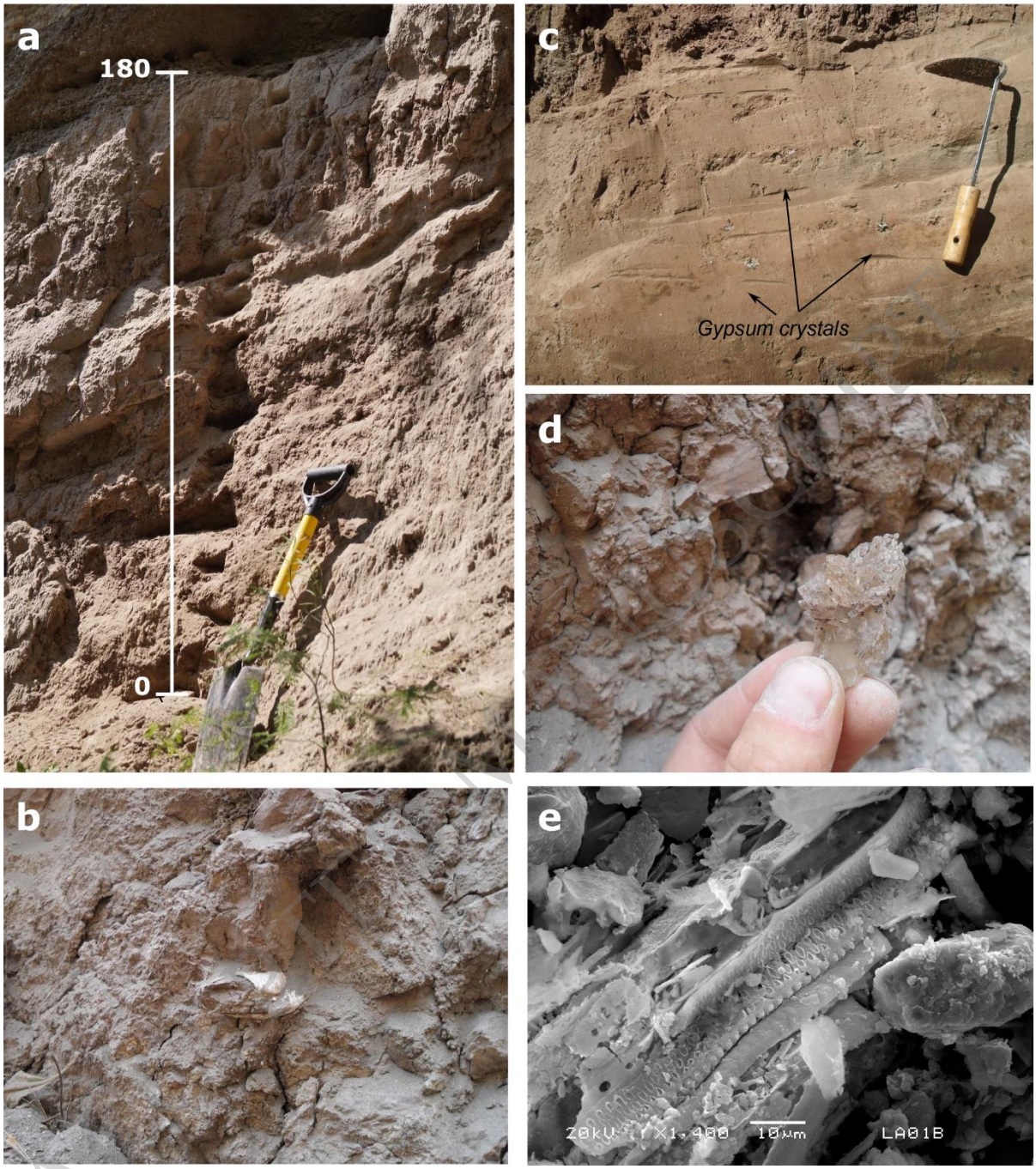

Figure 4

Downloaded from http://sp.lyellcollection.org/ at Universidad Nacional Autonoma De Mexico on August 24, 2021

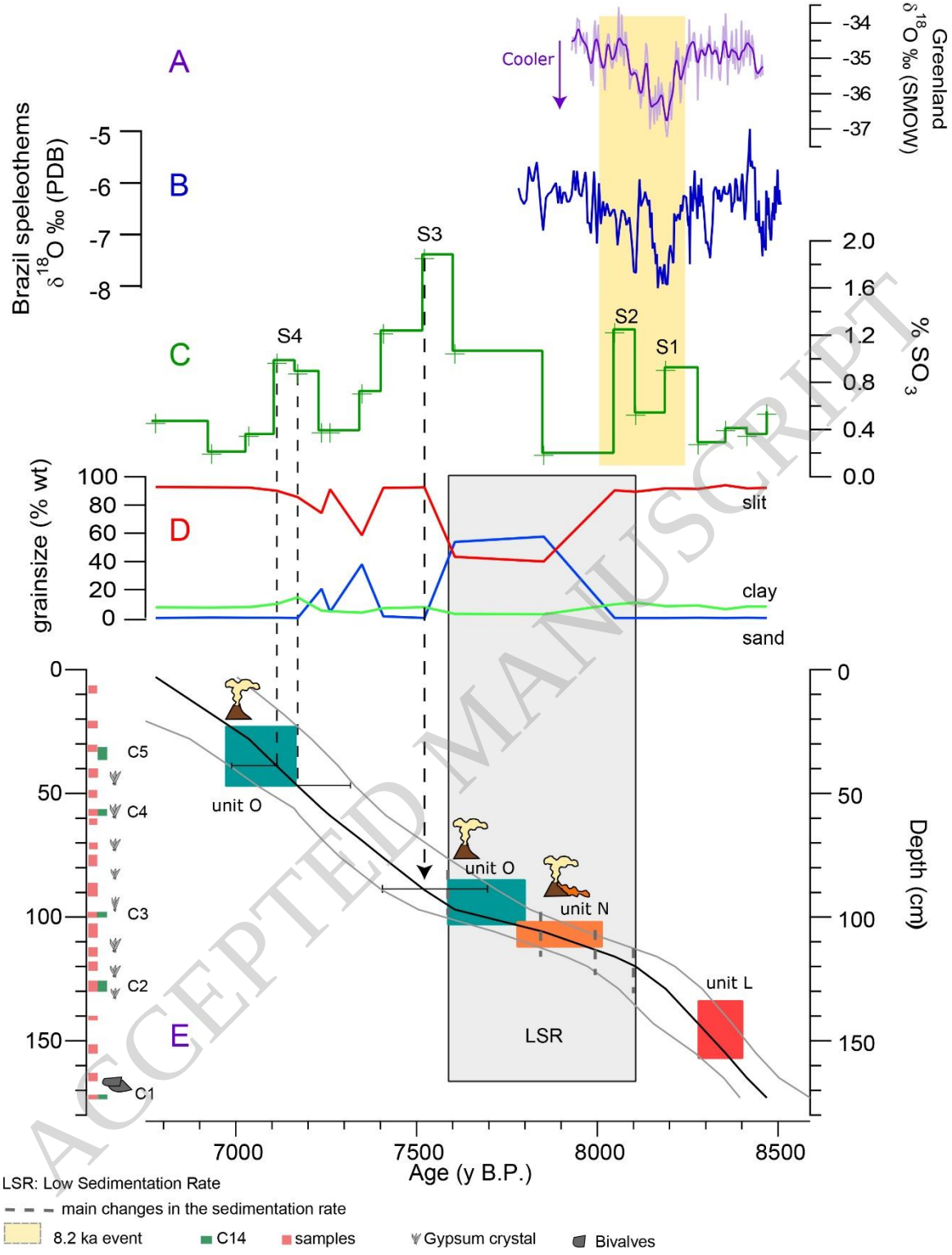

ACCEPTED MANUSCRIPT

Figure 5

Downloaded from http://sp.lyellcollection.org/ at Universidad Nacional Autonoma De Mexico on August 24, 2021

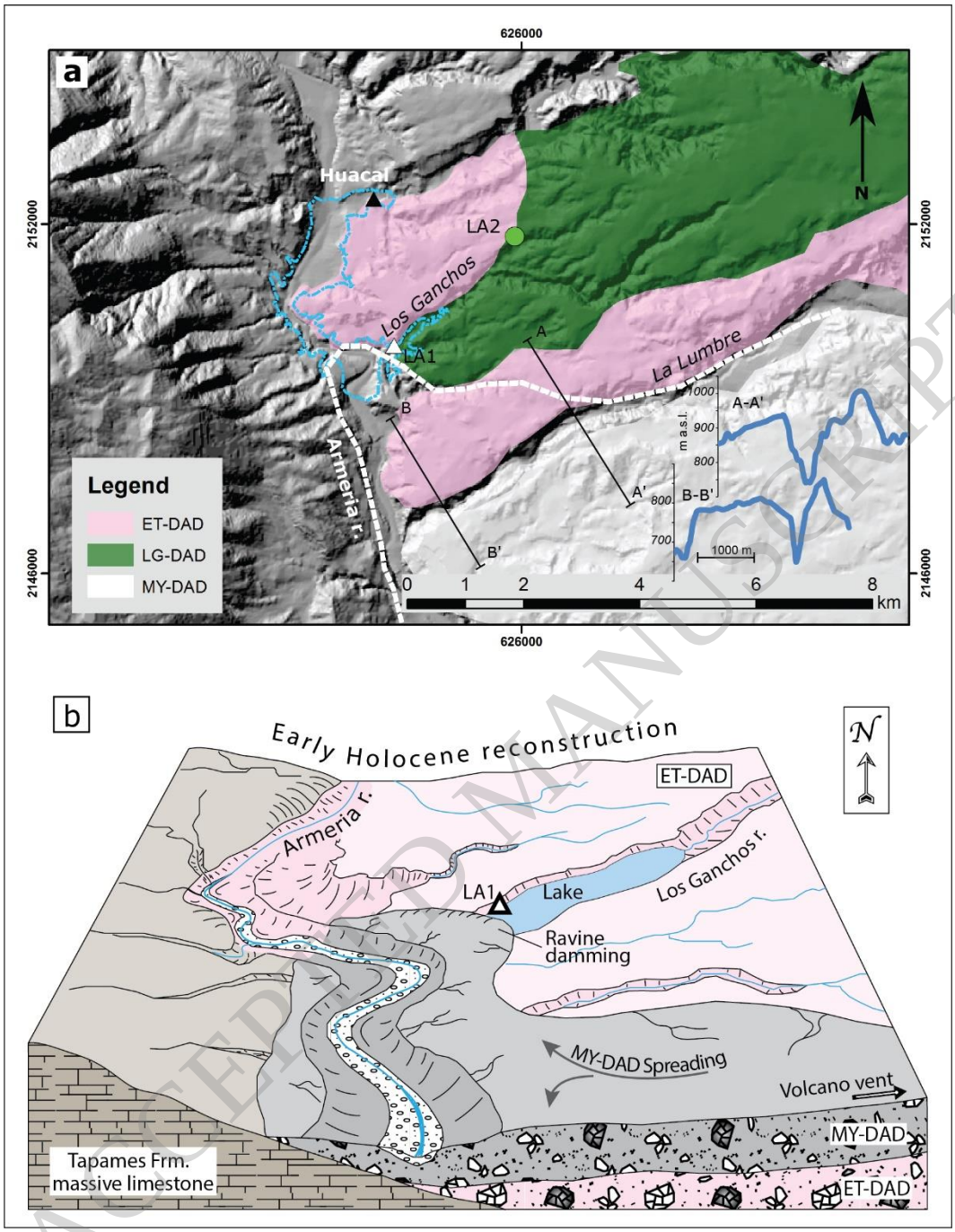

ACCEPTED MANUSCRIPT

Figure 6